Enzyme-Mediated Organic Neurohybrid Synapses

Antonio Lobosco, Claudia Lubrano, Daniela Rana, Viviana Rincon Montes, Simon Musall, Andreas Offenhäusser, and Francesca Santoro*

The development of organic artificial synapses that exhibit biomimicry features also may enable a more seamless integration of neuroelectronic devices in the nervous system, allowing artificial neuromodulation to be perceived as natural behavior by neuronal cells. Nevertheless, the capability to interact with both electroactive and non-electroactive neurotransmitters remains a challenge since state-of-the-art devices mainly rely on the oxidation of electroactive species. Here, the study proposes an organic artificial synapse engineered to enable interaction with non-electroactive species present in the central nervous system. By integrating a conductive polymeric film functionalized with platinum nanoparticles, the device can catalyze the oxidation of electroactive molecules (i.e., H_2O_2) resulting from neurotransmitter-specific enzymatic reactions following an enzymatic functionalization, therefore exhibiting neuromorphic functions driven by non-electroactive neurotransmitters. The creation of devices that can interact with or monitor these neurotransmitters can be seen as a significant step toward innovative technologies to expand the understanding of the mechanisms underlying neurological disorders and the development of novel, more effective treatments for them.

A. Lobosco, C. Lubrano, D. Rana, V. R. Montes, S. Musall,
A. Offenhäusser, F. Santoro
Institute of Biological Information Processing IBI-3
Forschungszentrum Juelich
52428 Jülich, Germany
E-mail: f.santoro@fz-juelich.de
A. Lobosco, C. Lubrano, D. Rana, F. Santoro
Neuroelectronic Interfaces
Faculty of Electrical Engineering and IT
RWTH
52074 Aachen, Germany
S. Musall
Institute of Biology 2
52074, RWTH Aachen Aachen, Germany
S. Musall
Faculty of Medicine
Institute of Experimental Epileptology and Cognition Research
University of Bonn
53127 Bonn, Germany

1. Introduction

Bioinspired electronics aims to mimic the structure and function of biological systems, such as the nervous system, using neuromorphic platforms and developing advanced smart materials.[1,2] Exoskeletons, prosthetics, and other devices that combine an electronic device with a living body are examples of bioinspired applications for which it seeks to develop electronic sensors and motor systems that mimic their biological counterparts.[3] These approaches are also relevant for engineering smart and adaptive neuroelectronic interfaces. The latter aims to monitor, stimulate, and modulate the neural activity to understand and restore neural functions.[4] However, their seamless integration with the nervous system from an electrochemical, physiological, and mechanical perspective is still a challenge. To face these limitations, not only material design (e.g., organic semiconductors) but an effective functional abiotic/biotic integration is needed.[5] This requires an interaction at the synaptic level, allowing devices to potentially adapt their response based on the electrochemical nature of the information process.[6] Here, a class of neuromorphic devices, organic artificial synapses, have been developed exploiting conductive polymers to perform mixed ionic-electronic conduction, in turn enabling electrochemical transduction.[7] In this manner, organic electrochemical transistors (OECTs) integrated as electrochemical neuromorphic organic devices (ENODes) have been developed.[8] They feature a three-electrode architecture metal–oxide–semiconductor field-effect transistor (e.g., MOSFET) with organic mixed ionic-electronic conductors (OMIECs) (e.g., PEDOT:PSS) as the channel material and an electrolyte at the gate/channel interface. Synaptic functions were reproduced in ENODes by applying pre-synaptic action potential-like voltage pulses at the gate electrode as a bias to facilitate the injection of ions from the electrolyte into the semiconductive channel and by recording the resulting post-synaptic channel current modulation as a function of time.[8,9] This results in both short- and long-term modulation of the electronic transport properties of the OMIEC structure, resembling the synaptic weight modulation of biological synaptic plasticity (e.g., short-term and long-term potentiation/depression in biological synapses). These neuromorphic systems can potentially generate electrical signals that are biocompatible and biomimetic, as well as provide an effective solution for on-chip computing, enhancing their integration in

ADVANCED
SCIENCE NEWS

www.advancedsciencenews.com

ADVANCED
MATERIALS

www.advmat.de

biological neural networks' information processing.[10] To date, PEDOT:PSS-based ENODes directly interfaced with living cells and capable of modulation of the channel's conductance level as a response to different concentrations of dopamine (DA, an important neurotransmitter in the central nervous system (CNS)) have been developed, resulting in a biohybrid artificial synapse with tunable synaptic weight and long-term potentiation[11] as well as achieving spiking organic neurons[6,12] and neurohybrid platforms with neuronal/neuromorphic functional interfaces.[13] These devices are sensitive to biologically relevant electroactive molecules (e.g., neurotransmitters and other biomarkers) with a non-selective approach, exploiting the oxidation reaction at the gate/electrolyte interface when a proper voltage is applied while more advanced synaptic models should be developed, allowing for selectivity, connectivity, and learning, and resembling the activity of other relevant non-electroactive neurotransmitters (e.g., glutamate, acetylcholine). Enzymatic functionalization at the gate electrode of OECTs has been proven to be an effective method to accomplish these requirements, leading, as a result of the enzymatic reaction, to key electroactive products, such as hydrogen peroxide (H_2O_2).[14] These species can be exploited for channel current modulation when oxidized through gate electrode stimulation. Principles of this kind have been extensively applied in the development of enzymatic electrochemical biosensors based on OECT architecture.[15,16] Nevertheless, H_2O_2 effects on PEDOT:PSS-based ENODes have been used to restore the channel conductance level after modulation mediated by neurotransmitter oxidation, enabling a closed control system.[17] However, it is still important to evaluate the effect of H_2O_2 oxidation-associated neuromorphic functionalities[18] (e.g., long-term plasticity) and how, acting as a synaptic modulator, it could enable artificial synapses' response to non-electroactive species.

Here, we present an engineered PEDOT:PSS-based ENODe as an artificial synapse functionalized with Pt nanoparticles that exhibits neuromorphic functions owing to Pt electrocatalytic activity toward H_2O_2 oxidation, resulting in both short-term and long-term modulation of the channel's conductance level. Next, we focused on creating an enzyme-based artificial synapse with a tunable synaptic weight and long-term plasticity through the interaction with non-electroactive neurotransmitters, exploiting electrochemical detection of H_2O_2 resulting from the reaction with a neurotransmitter-specific oxidoreductase enzyme (i.e., L-GlutOx). This work paves the way to creating neurohybrid synapses that exploit a versatile enzymatic-based modulation that can be potentially applied to diverse non-electroactive neurotransmitters and molecules that play key roles in synaptic signal transmission and plasticity.

2. Results and Discussion

2.1. Development and Characterization of Pt NPs-Functionalized ENODe

ENODes based on a three-terminal architecture including a gate electrode (i.e., presynaptic terminal) and a semiconductive channel (i.e., postsynaptic terminal) connecting the drain and source electrodes were engineered to emulate the neurochemical signal processing of biological synapses. The fabrication process

details are reported in the Experimental Section. In particular, the gate electrode was obtained by spin coating a thin layer of PEDOT:PSS further functionalized with Pt nanoparticles (NPs) to immobilize an enzyme to selectively bind non-electroactive molecules (i.e., glutamate) (**Figure 1a**). The Pt NPs electrodeposition was achieved via cyclic voltammetry (CV) from a precursor solution (Figure S1, Supporting Information, Experimental section).[19] Pt NPs were successfully embedded in the 3D matrix of the PEDOT:PSS film after fifteen CV cycles (Figure S1b, Supporting Information, Experimental section). The presence and the morphology of the particles on samples electrodeposited with 10, 15, and 20 CV cycles were confirmed and analyzed through scanning electron microscopy (SEM), while optical spectrometry was also performed to assess the film's transparency. Transmittance measurements comparing samples before and after fifteen CV cycles of electrodeposition are reported in Figure 1b. SEM analysis confirmed that the increasing number of CV-based electrodeposition cycles directly correlated to a higher number of Pt NPs being deposited into the film and to the formation of particle clusters (Figure S1c–e, Supporting Information). Notably, optical spectrometric analysis showed that after 20 electrodeposition cycles the film transparency was not preserved, whereas 15 electrodeposition cycles supported a homogeneous distribution of Pt particles within the film while partially maintaining the gate electrode transparency. Then, the electrocatalytic activity of the PEDOT:PSS/Pt NPs composite film was then assessed by means of CV performed in 1 mM H_2O_2 solution in DPBS (Experimental section). The functionalized gate exhibited H_2O_2 oxidation and reduction characteristic peaks at ∼ +0.25 V and –0.25 V, respectively (Figure 1c), that confirm the interaction with the Pt nanoparticles, as also reported in previous studies.[14] In contrast, no peaks were observed in the same potential range in the case of bare PEDOT:PSS films, as no electrochemical interaction with H_2O_2 was observed (Figure 1c). Moreover, oxidation peaks current increased with higher electrodeposition cycles, suggesting that a higher density of nanoparticles at the gate electrode could more effectively oxidize H_2O_2 (Figure S2a, Supporting Information). Finally, considering the electrochemical, morphological, and transparency properties, the composite films obtained with 15 cycles were the most suitable as gate electrodes, showing reproducible H_2O_2 detection (N = 3, Figure S2b, Supporting Information).

2.2. ENODe Electrical and Electrochemical Characterization

Output curves showed a channel current (I_{DS}) modulation as the applied gate voltage (V_{GS}) was increased from –0.2 to 0.8 V, both with and without H_2O_2 in the electrolyte (Figure 1d). In comparison to the case where the electrolyte was solely DPBS, a greater I_{DS} modulation was observed when the synaptic modulator was present (Figure 1d, dashed lines). This suggests that H_2O_2 oxidation at the gate electrode produced protons that were driven through the electrolyte toward the PEDOT:PSS channel, causing further de-doping of the polymer. This was consistent with previous findings where protons were produced by oxidizing an electroactive molecule at the gate electrode in PEDOT:PSS-based OECTs.[20] Furthermore, the transconductance was extracted from the transfer curves,[21] obtained at different H_2O_2
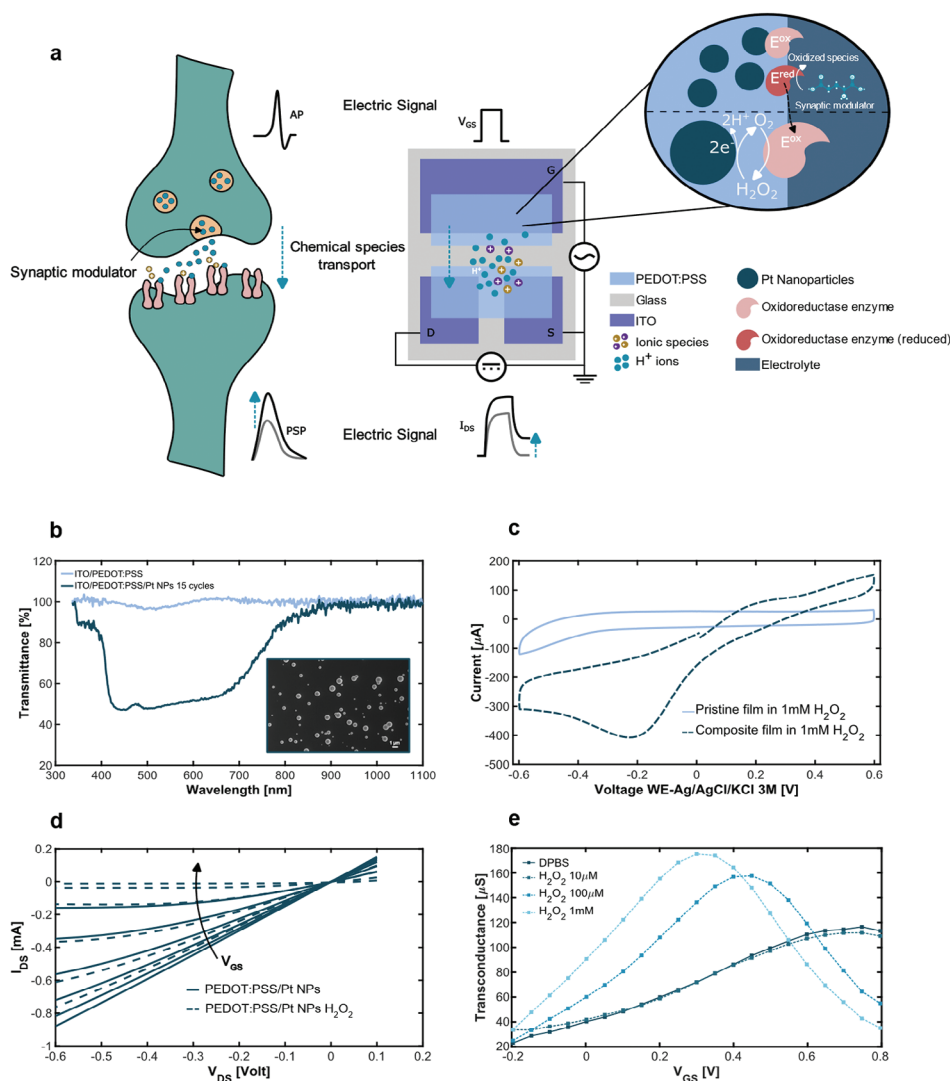
2409614 (2 of 10)

**ADVANCED
SCIENCE NEWS**

www.advancedsciencenews.com

**ADVANCED
MATERIALS**

www.advmat.de

Figure 1. Enzyme-functionalized ENODe's structure and functioning. a) Schematic of the ENODe function emulating the signal processing of a biological synapse with a presynaptic stimulation occurring at the gate electrode functionalized with Pt NPs and the neurotransmitter-specific enzyme and a postsynaptic response that occurs at the semiconductive channel. The channel current modulation, which is driven by the protons obtained from the enzymatic reaction at the gate electrode, is highlighted. b) Optical spectrometric measurements of the PEDOT:PSS film before and after the electrodeposition of Pt NPs showing the partial preservation of PEDOT:PSS transparency after the functionalization with 15 cycles. SEM image showing the composite film morphology. c) Cyclic Voltammetry of pristine PEDOT:PSS film before (continuous line) and after functionalization (dashed line) when H_2O_2 is added to the electrolyte and in the same voltage window. It shows the presence of current peaks related to the H_2O_2 redox reactions. d) Output curve of the Pt NPs-functionalized ENODe in DPBS (continuous line) and 1 mM H_2O_2 (dashed line), showing the higher channel current depletion in H_2O_2 solution as the V_{GS} value increases from −0.2 to 0.8 V. e) Transconductance values obtained from the transfer curves measured in DPBS (continuous line) and at three different H_2O_2 concentrations.

concentrations (Figure S2c, Supporting Information). As the analyte concentration increased, the number of oxidation events at the gate electrode also increased, which could further reduce the hole density in the channel. Furthermore, an increase in the analyte concentration can raise the effective voltage by altering the voltage drop across the electrolyte due to faradaic processes occurring at the gate electrode.[22] As a result, the gate voltage bias required to modulate the channel current (i.e., depletion) to a specific level decreases with higher analyte concentrations at the gate/electrolyte interface. This resulted in a shift of the transconductance peak toward zero gate-source voltage and an increase in

transconductance peak values (Figure 1e). Then, to characterize the transient response of the device for neuromorphic applications, a long-lasting quadratic voltage pulse was applied to the gate electrode when the analyte was added to the electrolyte. The devices were continuously biased and monitored for 1800 s, reflecting the inherent stability of Pt-functionalized devices under aqueous conditions.

Prior to the Pt NPs functionalization, no difference in channel current response was observed before and after the addition of the analyte in the electrolyte solution (Figure S2e, Supporting Information). Finally, a calibration curve has been
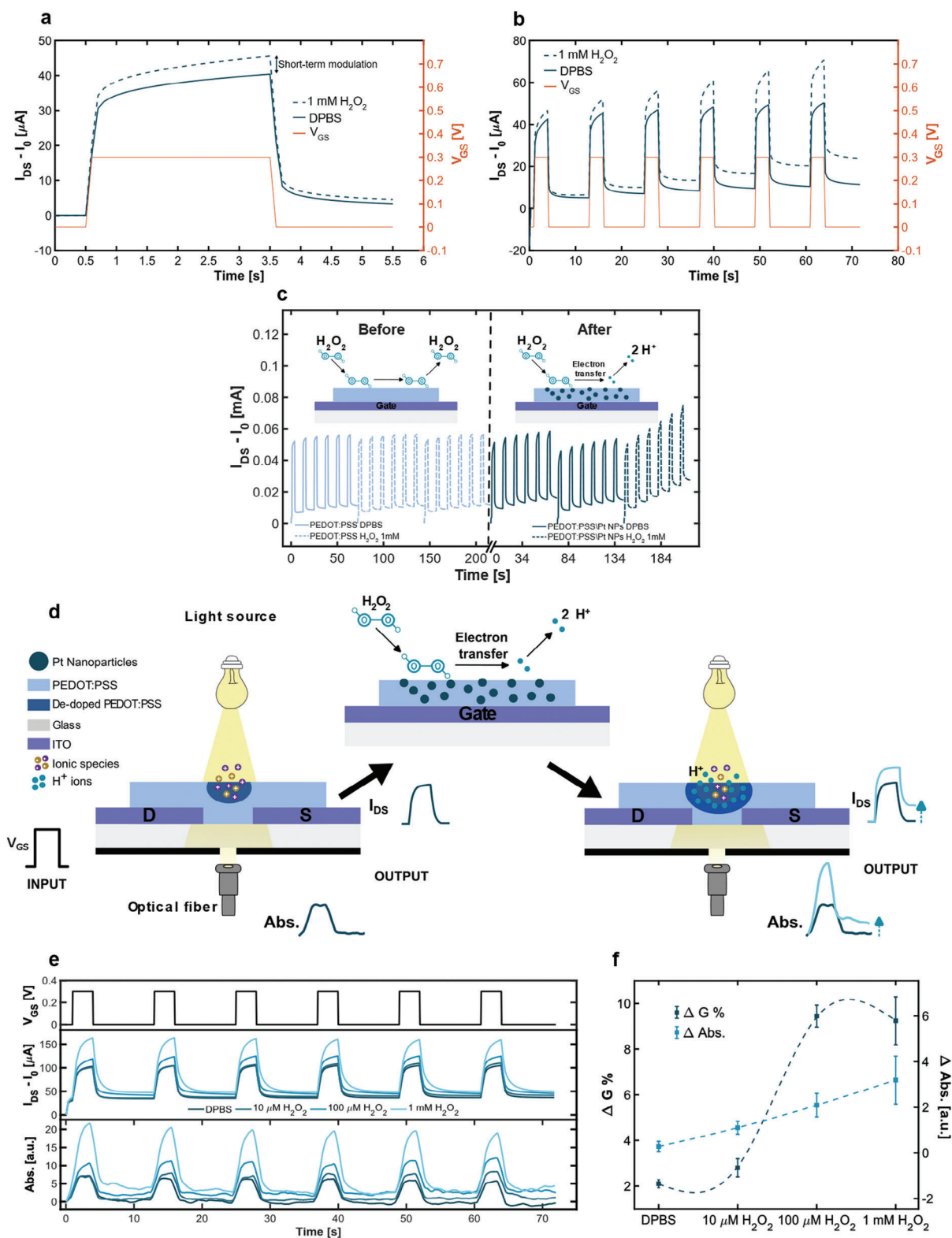
ADVANCED
SCIENCE NEWS

www.advancedsciencenews.com

ADVANCED
MATERIALS

www.advmat.de

Figure 2. ENODe's opto-electronic neuromorphic operation. In all measurements, the first value of the channel current, denoted with I_0, was subtracted from the I_{DS} to compare devices with different baseline currents. a) Channel current response to a single voltage pulse, highlighting short-term modulation during the on-phase of the voltage pulse. b) Channel current response to sequential voltage pulses, showing long-term modulation in terms of non-reversible current baseline modulation. c) The response of the same ENODe to sequential voltage pulses before and after Pt NPs functionalization. Device response was monitored in the case of bare electrolyte (continuous curves) and in 1 mᴍ H_2O_2 solution (dashed curves) before and after the

2409614 (4 of 10)

ADVANCED
SCIENCE NEWS

www.advancedsciencenews.com

ADVANCED
MATERIALS

www.advmat.de

extracted from the measurements carried out at different analyte concentrations, indicating the capability of a significant response to H_2O_2 concentrations in the order of hundreds of nanomolar (≈ 300 nM) (Experimental section and Figure S2f, Supporting Information) which is relevant also for the further functionalization with the enzyme and its specific H_2O_2 production upon analyte binding.[23,24]

2.3. Opto-Electronic H_2O_2-Driven Neuromorphic Activity

Then the operation of the artificial synapse was investigated considering the response to H_2O_2 and its possible effect on the short-term modulation of the channel current and long-term plasticity induced in the ENODe upon the application of periodic voltage pulses at the gate electrode to emulate presynaptic stimulation, while applying a constant negative voltage between drain and source terminals. The amplitude of V_{GS} was set to 0.3 V, a slightly higher value than the overpotential related to the oxidation peak observed from the CV analysis, ensuring H_2O_2 oxidation. **Figure 2a** reports the I_{DS} response to a single voltage pulse of a Pt NPs-functionalized device, highlighting a higher pulse amplitude (i.e., current depletion) in the presence of H_2O_2 than the solely DPBS solution case. This modulation could only be observed during the on-phase of the voltage pulse, that is, in the presence of the presynaptic stimulus, demonstrating short-term modulation of the ENODe's synaptic weight. Long-term modulation is then depicted in Figure 2b, highlighting reversible and non-reversible I_{DS} baseline modulation following V_{GS} pulses (consisting of six squared pulses with 3s duration and 9s delay between pulses,[17] Experimental Section) in DPBS and 1 mM H_2O_2 (dashed lines) solutions, respectively. These measurements were repeated on the same device before and after Pt NPs functionalization in DPBS (continuous line) and 1 mM H_2O_2 (dashed lines) to demonstrate Pt NPs-enabled neuromorphic activity in response to H_2O_2 when the same presynaptic stimuli were applied (Figure 2c). H^+ ions and electrons generated during the faradaic reaction at the gate electrode in the presence of H_2O_2 had a high impact on the non-reversible channel current modulation. The H^+ ions injected into the PEDOT:PSS channel form stable sulfonic acid groups by bonding with the PSS-, in contrast to the injected electrolyte cations, which can gradually diffuse back into the electrolyte solution once the voltage stimulus is removed.[11,25] The non-reversible channel current modulation depended on the analyte concentration in the electrolyte solution and the corresponding number of cations injected from the gate and retained in the neuromorphic channel during the application of the pulsed gate bias (Figure S3a,b, Supporting Information). Simultaneously with the electric measurements, time-resolved UV-vis measurements were performed to moni-

tor the local absorbance variation at the channel terminal and to demonstrate opto-electronic neuromorphic activity exploiting the PEDOT:PSS electrochromic nature (Figure 2d).[26] The reference intensity spectrum was acquired when V_{GS} was set to zero and the channel was doped, then the absorbance at the wavelength corresponding to the intensity peak was tracked over time during the pulsed measurements (Experimental Section). An absorbance increase was observed as a result of the polymer electrochemical de-doping during device operation under a white light source, as also previously reported.[27] The opto-electronic response to a series of periodic voltage pulses is shown in Figure 2e, where at the V_{GS} pulse, the channel current exhibited a depletion with a simultaneous local variation of absorbance as a result of the polymer de-doping process. From these considerations, absorbance and channel conductance variations (ΔAbs. and ΔG%, respectively) were chosen as parameters for the artificial synapse weight modulation, therefore used to characterize the H_2O_2-driven neuromorphic activity (Figure 2f). An increase in the H_2O_2 concentration from 10 to 100 µM led to higher variations in absorbance (1.14 a.u. to 2.1 a.u., respectively) and conductance (2.8% and 9.43%, respectively). Interestingly, when the concentration reached 1 mM value, no further increases could be observed, indicating either the possibility of a competing effect taking place at high H_2O_2 concentrations due to a reoxidation of the channel polymer by the remaining non-oxidized H_2O_2,[17] or a channel saturation effect.

2.4. Glutamate-Based Artificial Synapse

Following the study and characterization of Pt NPs-functionalized ENODes response to H_2O_2, its function as synaptic modulator mediating neuromorphic operations in response to non-electroactive molecules was assessed. Here, glutamate binding at the gate electrode was achieved through a chitosan-based enzyme immobilization on the PEDOT:PSS/Pt NPs film (Experimental Section and Figure S4, Supporting Information). The electrochemical detection was obtained by means of an oxidoreductase enzyme,[14,29] namely L-Glutamate Oxidase (L-GlutOx) (**Figure 3a**). The enzymatic reaction process is described by the following equation: $L - glutamate + O_2 + H_2O \rightleftharpoons 2 - oxoglutarate + NH_3 + H_2O_2$.

Glutamate was oxidized to 2-oxoglutarate, reducing the enzyme, which was subsequentially re-oxidized by the oxygen. H_2O_2 was then formed following oxygen reduction and enzyme re-oxidation, leading to the electroactive synaptic modulator. Additional details on the enzymatic reaction process and the general working principle of the device are reported in Figure S5 (Supporting Information). The amount of H_2O_2 produced over time is directly proportional to the amount of glutamate oxidized

---

functionalization, showing a clear long-term modulation of the baseline current only in the case of the functionalized device operating in presence of the synaptic modulator. d) Schematic of ENODe's opto-electronic operation under optical illumination while the optical fiber records the light transmitted through the electrochromic post-synaptic terminal. From left to right: the post-synaptic response when H_2O_2 is not present at the gate/electrolyte interface; the electrochemical reaction occurring at the gate electrode when H_2O_2 is present in solution and the H^+ resulting from the Pt-catalyzed H_2O_2 oxidation reaction; the enhanced post-synaptic response due to the H^+-related polymer de-doping at ENODe's channel (the darken region highlights a further de-doping). e) Opto-electronic measurements when sequential voltage pulses are applied. From top to bottom: presynaptic stimulation (V_{GS} pulses); channel current time-response and related absorbance changes extracted from monitoring the light transmitted through the post-synaptic terminal during ENODe electrical operation in DPBS and at different H_2O_2 concentrations. f) Absorbance and conductance variations at different H_2O_2 concentrations, quantifying post-synaptic long-term modulation.

**ADVANCED
SCIENCE NEWS**

www.advancedsciencenews.com
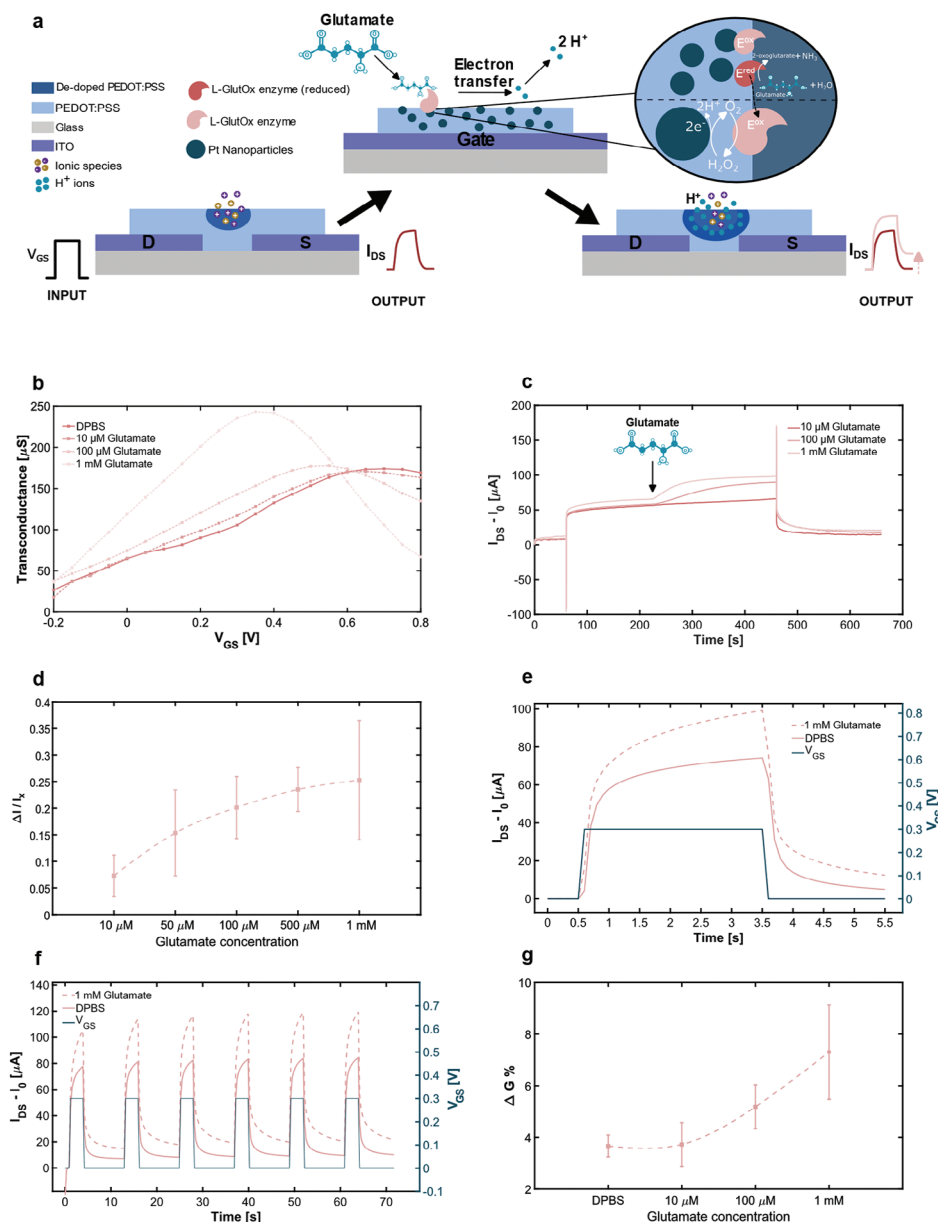
**ADVANCED
MATERIALS**

www.advmat.de

Figure 3. Glutamate-driven neuromorphic functions of the enzyme-functionalized ENODe. a) Schematic of the enzyme-functionalized ENODe post-synaptic response when a pre-synaptic stimulus occurs. From left to right: the post-synaptic response when glutamate is not present at the gate/electrolyte interface; the mechanism of the enzymatic reaction occurring at the gate electrode when glutamate is present in solution and the H^+ resulting from the Pt-catalyzed H_2O_2 oxidation reaction; enhanced post-synaptic response due to the H^+-related polymer de-doping at ENODe's channel (the darkened region highlights a further de-doping). b) Transconductance values of the enzyme-functionalized ENODe obtained from the transfer curves measured in DPBS (continuous line) and in three different glutamate concentrations. c,d) Long-lasting pulse response when glutamate is added in the electrolyte solution at 220 s, showing further depletion of the channel current at different glutamate concentrations and related current depletion quantification, respectively (capacitive peaks at the onset and the offset of the pulse were not filtered). e) Channel current response to a single voltage pulse, highlighting short-term modulation during the on-phase of the voltage pulse. f) Channel current response to sequential voltage pulses, showing long-term modulation in terms of non-reversible current baseline modulation when glutamate is present in the electrolyte solution. g) Error bar plot of conductance variations at different glutamate concentrations, quantifying post-synaptic long-term modulation.

during the enzymatic reaction.[14] Therefore, the amount of enzyme units immobilized at the electrode surface constitutes a key parameter to optimize sensing performances. Nevertheless, while important for biosensing applications, it was deemed less critical for understanding and optimizing the overall performance of the artificial synapse in mimicking synaptic functionalities. Output and transfer curves were obtained in DPBS before and after enzyme immobilization at the gate electrode (Figure S6a,b, Supporting Information), showing higher channel current modulation when the enzyme was immobilized, suggesting that the formation of an additional non-conductive layer resulted in an increase in the gate electrode capacitance.
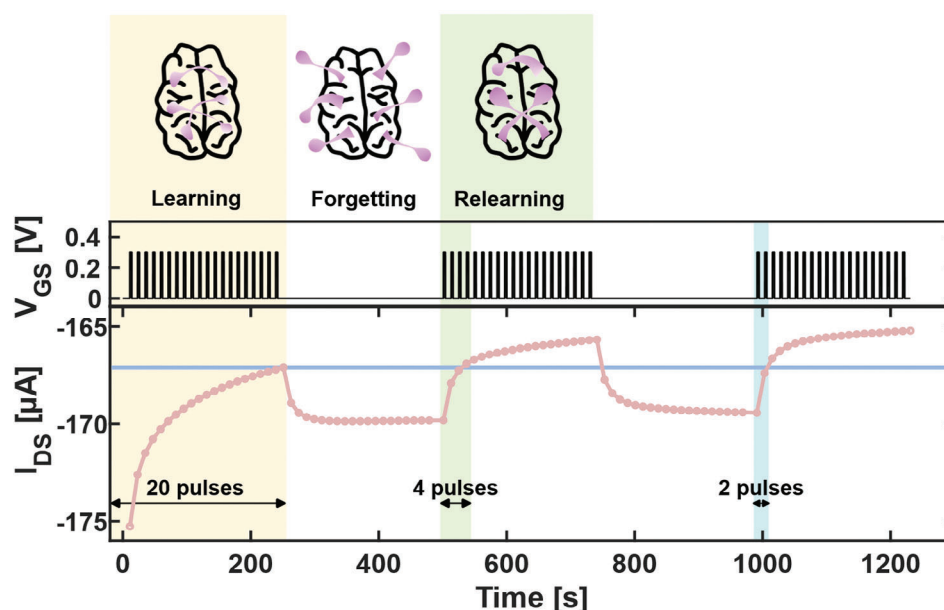
**ADVANCED
SCIENCE NEWS**

www.advancedsciencenews.com

**ADVANCED
MATERIALS**

www.advmat.de

Figure 4. ENODe mimicking biological learning-forgetting process. The channel current was monitored during ENODe operation in 1 mm glutamate solution by considering, for each point, the current values taken at the end of each pulse (pink curve). The blue line represents the learning threshold that is reached by the ENODe at the end of the learning phase. Fresh glutamate solution was added in the microfluidic channel at the end of each forgetting phase.

The ENODe was then exposed to different glutamate concentrations (10 μm, 100 μm, 1 mm) (Figure S6c,d, Supporting Information) and the related transconductance curves were then obtained (Figure 3b), exhibiting a peak shift toward lower V_{GS} values, from +0.7 V to +0.35 V, as the concentration increased. Furthermore, the I_{DS} response to a single long-lasting squared voltage pulse was monitored by adding glutamate to the electrolyte solution at ≈220s after the I_{DS} value stabilized (I_x, Figure 3c). The measurements performed at different glutamate concentrations are shown in Figure 3d. When glutamate was added to the electrolyte solution, a further depletion in the channel current was observed, and the entity of the depletion increased with concentration, indicating the effective glutamate-sensing capabilities of the device.

The glutamate-driven neuromorphic activity was then evaluated based on these factors, investigating both short-term and long-term modulation at different glutamate concentrations as response to presynaptic stimuli, consistently with the previous characterization with H_2O_2. Exemplary results related to 1 mm glutamate concentration are shown in Figure 3e,f, depicting short-term and long-term I_{DS} modulation, respectively. The conductance percentage variations were then extracted from these measurements, indicating an increase by increasing glutamate concentrations and reflecting the effective neuromorphic operations capabilities of the device despite the limited sensing performance since no significant response was recorded at 10 μm glutamate concentration (Figure 3g). Although this represents a limitation for operating this proof-of-concept device at physiological concentrations, the sensing capabilities were sufficient to analyze glutamate-driven neuromorphic functioning.

2.5. Mimicking Biological Learning-Forgetting Process

As mentioned earlier, in biological synapses, sustained presynaptic stimulation can result in an increased neurotransmitter release, which in turn can lead to an increase in receptor density at the postsynaptic membrane, enhancing the neuronal responsiveness to subsequent signals.[30] Similarly, in depletion-mode ENODes, the application of a positive gate-source voltage induces a modulation in the conductive polymer that can be associated with the synaptic plasticity, the basis of the biological learning process. This voltage application causes a reduction in the number of available electronic charge carriers, effectively depleting the channel's conductivity. Here, glutamate-based learning, including forgetting and relearning processes, was achieved. A sequence of 20 squared voltage pulses was applied at the gate electrode in the presence of 1 mM glutamate solution (**Figure 4**). After the initial sequence of pulses, referred to as the learning phase, the channel current measured at the end of each pulse increased, reaching a level considered the learning threshold. Following this, during the forgetting phase, where no presynaptic stimuli were applied, the channel current gradually decreased below the threshold. Prior to the application of another presynaptic stimuli sequence, 1 mM glutamate solution was inserted into the microfluidic channel, hence constituting the relearning phase. In this phase, only four pulses were required to achieve the learning threshold. Another cycle of forgetting and relearning was performed, this time achieving the learning threshold after only two pulses. A human brain relearns a forgotten memory faster than a new memory; this ability has "time-saving" effects.[31] In this experiment, the amount of stimulation to attain the same synaptic weight (i.e., channel current level) was lower during

2409614 (7 of 10)

**ADVANCED
SCIENCE NEWS**

www.advancedsciencenews.com

**ADVANCED
MATERIALS**

www.advmat.de

relearning than during the first learning process; therefore, forgotten information can be relearned easier than new information also in the here proposed artificial synapse, resembling biological learning processes.[32] Notably, the incomplete recovery of the initial channel conductance level was pivotal to ensuring this biomimetic functioning. Although, providing H_2O_2 without oxidizing it could restore the channel conductance level after modulation mediated by neurotransmitter oxidation,[17] potentially resembling memory loss. These systems can exhibit a form of adaptability: neurons through the regulation of receptor numbers and ENODes through the modulation of charge carrier density, highlighting the inherent flexibility and dynamic nature of both biological and synthetic organic materials in response to environmental changes.

3. Conclusion

This work presents an organic artificial synapse based on an enzyme-functionalized ENODe architecture that exhibits glutamate-driven neuromorphic functionalities. However, these findings suggested the possibility of developing ENODes able to respond to other relevant non-electroactive neurotransmitters, such as acetylcholine, by integrating neurotransmitter-specific enzymatic reactions producing key electroactive molecules (e.g., H_2O_2). We proved how a functionalization of PEDOT:PSS with Pt NPs at the gate terminal of the device, together with its electrochemical and morphological characterization, enabled both sensing and opto-electronic neuromorphic functions in the presence of H_2O_2, highlighting the capabilities of this molecule to function as a synaptic modulator. Moreover, the proposed ENODe exhibited neuromorphic functions, mimicking synaptic information processing in response to glutamate after neurotransmitter-specific enzyme immobilization at the gate electrode. Ultimately, considering its crucial role in memory and cognitive functions,[33] an experiment involving learning, forgetting, and relearning processes was carried out in the presence of the neurotransmitter, emulating the relearning phase of forgotten information associated with human memory processes.

4. Experimental Section

ENODe Fabrication: Devices were fabricated through spin coating of a PEDOT:PSS aqueous solution. The solution was prepared using 94% vol commercial PEDOT:PSS Clevios PH 1000, 5 vol.% ethylene glycol (EG), 1 vol.% 3-glycidyloxypropyl-trimethoxysilane (GOPS), and 0.02 vol% dodecylbenzene sulfonic acid (DBSA), all purchased from Sigma-Aldrich.

Patterned glass substrates (25 × 25 mm) with two squared pads (10 × 10 mm) of Indium Tin Oxide (ITO) at each corner on one side, and a third pad (13 × 25 mm) on the other side, were obtained from KinTek (KT21007). These substrates were used for device fabrication via rapid prototyping, involving selective masking and spin coating, followed by a final annealing step to enhance stability and conductivity.

Prior to spin coating, each glass was covered with Kapton tape. A 3D-printed stencil-like guide was then used to expose two parallel stripes (17 × 7 mm, 1.5 mm apart) of glass/ITO surface using a bistoury. These exposed areas allowed the PEDOT:PSS to form the gate electrode and the corresponding semiconductive channel of the ENODe. The masked glasses were rinsed with deionized water and 2-propanol, dried with a nitrogen gun, and subjected to O2 plasma activation and cleaning (5 min, 100 W) to facilitate spin coating.

The PEDOT:PSS solution was sonicated for 10 minutes before use. The samples were spin-coated at 2000 rpm for 1 minute with an acceleration of 400 rpm s^{-1} and then annealed at 140 °C for 1 hour. After the spin coating and annealing process, the Kapton tape mask was mechanically removed, leaving the two PEDOT:PSS film stripes on the substrate.

Device Functionalization with Platinum Nanoparticles: Pt nanoparticles (Pt NPs) were electrochemically deposited into the PEDOT:PSS matrix at the gate electrode using the cyclic voltammetry (CV) technique. This was performed with a CHI Instrument 1030B potentiostat and a solution of hexachloroplatinic acid (H_2PtCl_6) in an electrochemical cell. A stripe of Kapton tape was attached to prevent nanoparticle electrodeposition on the exposed ITO at the gate electrode and within the cavity of a glass ring (diameter: 17 mm, height: 10 mm) used to contain the electrodeposition solution. The glass ring was positioned to ensure that the plating solution (900 µl) did not contact the PEDOT:PSS stripe of the device's channel during electrodeposition.

A bistoury was used to expose a small portion of ITO in a corner of the glass, onto which silver paste was deposited to provide good contact with the working electrode connection of the potentiostat. Before placing the glass ring on the device's surface, biphasic glue was applied to the bottom border of the ring. The ring was then placed on a clean glass and cured on a hot plate at 120 °C for at least 2 minutes to form a sealed ring, preventing solution leakage during the electrodeposition process. A plating solution of 5 mM H_2PtCl_6 8 wt.% in water, 0.01 M HCl, 0.1 M KCl (pH 1.73) was used and prepared right before electrodeposition of each sample at room temperature.[19] CV was employed to deposit Pt particles by cycling the potentials (versus Ag/AgCl/3 M KCl reference electrode, Redox.me) between −0.25 and 0.8 V for 15 cycles with a scan rate of 50 mV s^{-1}. After Pt particles incorporation, the electrode was rinsed with double-distilled water for 5 min and dried at 150 °C on a hotplate for 3 min. After this process, a PEDOT:PSS/Pt NPs composite film was obtained. The optimal number of electrodeposition cycles (i.e., 15) was found performing morphological, electrochemical, and spectrometric analysis of the composite film resulting from 10, 15, and 20 electrodeposition cycles.

Device Functionalization with Chitosan-Based L-Glutamate Oxidase Enzyme Immobilization: For preparing the functionalization of the gate electrode, a chitosan film was electrodeposited with CHI Instrument 1030B potentiostat at −1.0 V versus Ag/AgCl for 2 min (repeating for 2 more times) on the areas targeted for glutamate oxidase immobilization.[28,29] A 50 ml Acetic Acid pH = 3.05 electrodeposition solution was obtained by adding 161.86 µl of Acetic Acid (Sigma Aldrich ≥99%) to 49.84 ml of MilliQ water. Then 10 ml of this solution was added to 8 mg of Chitosan (Sigma Aldrich, medium MW, DD 75–85%) to obtain a 0.08% m/V chitosan solution in a 20 ml glass vial, and magnetic stirring was performed at 50 °C, 800 rpm, for at least 1.5 hours. A two-component mold was fabricated to obtain a membrane with a rectangular aperture available for gate electrodeposition with Chitosan in a limited area of the gate (7 mm x 4 mm) and a ring-shaped guide to avoid the chitosan solution leakage from the glass ring positioned on the top of the membrane. For the immobilization, 12.5 µl 0.2U/µl enzyme solution was drop-cast on the Chitosan/Pt-functionalized gate electrode area by a PDMS well, right after chitosan electrodeposition. Then the device was placed in a petri dish, sealed with parafilm to prevent evaporation of the enzyme solution, and stored in fridge for 8 hours at +4 °C. 3. A solution based on Bovine Serum Albumin (BSA) (ThermoFisher (gibco)) and Gluteraldehyde (GTA) (Sigma-Aldrich) solution was prepared following this procedure: 1% w/v BSA solution in water was obtained by mixing 10 mg of BSA in 1 ml of MilliQ water; then 50% w/w GTA in water was diluted to obtain 10 µl 25% w/w solution; the BSA and GTA solutions were mixed and let to crosslink for 5 min. Subsequently, 12.5 µl of the GTA/BSA solution was added to the enzyme-functionalized gate surface as a protective layer, and the device was left to dry overnight at room temperature. Before any reported measurement, the device was gently rinsed with DI water to remove any non-immobilized enzyme. The devices were then stored in the fridge at +4 °C in the same petri dishes with DI water placed in the microfluidic channel to avoid enzyme denaturation and sealed with parafilm.

Morphological Characterization: The morphological and topological characterization of the PEDOT:PSS/Pt NPs composite film was conducted

**ADVANCED
SCIENCE NEWS**

www.advancedsciencenews.com

**ADVANCED
MATERIALS**

www.advmat.de

using scanning electron microscopy (SEM). No additional conductive film coating was needed, as the ITO-coated glass and Pt nanoparticles form an interconnected electron path between the polymer microstructure and the conductive ITO layer underneath, allowing for direct imaging.

To enhance contact with the film and ensure efficient charge flow to ground, a small amount of silver conductive paste was applied to a corner of the sample, which was then secured to the SEM stage with a metallic clamp. A field emission SEM (FE-SEM Leo 1550 ZAT, Carl Zeiss Microscopy GmbH) was used, operating at an EHT of 10.00 kV with a 30.00 μm aperture size and an In Lens detector. Imaging was performed under vacuum conditions, with magnifications ranging from 10 kX (for statistical evaluations of particle size distribution and density) to 300 kX (for particle morphology).

Optical Spectrometric Analysis: Spectrometric analysis was performed to assess the film's transmittance after the electrodeposition process. The measurements were performed by means of customized software installed on the commercial platform measurement system, ARKEO (Cicci Research S.r.l.). It had the possibility to magnetically fasten an optical fiber beneath its stage in a position extremely close to the sample. A 12-led lamp (used as the white light source) was positioned on top of the stage where the sample was placed. A stage aperture (5 mm × 5 mm) located between the sample and the optical fiber allowed light to pass through the sample and to be recorded by the optical fiber. Clean ITO glasses provided the intensity reference values for the transmittance of ITO/PEDOT:PSS and Pt-functionalized samples.

Electrochemical Characterization: Experiments were carried out in a three-component cell employing a CHI instrument, Inc. VSP-300 potentiostat. An Ag/AgCl/3 M KCl glass electrode (Redox.me), coiled Pt wire, and an ITO-coated glass plate (17 × 20 mm, Ossila Ltd., S111) were used as reference, counter, and working electrodes, respectively. After PEDOT:PSS coating and thermal annealing, a glass ring (diameter: 17 mm, height: 10 mm) was attached to the ITO coated glass with a biphasic glue (Picodent, eco-sil, Dental Produktions-und-Vertriebs-GmbH) that sealed the ring and substrate, preventing electrolyte leakage. To enhance the contact between the sample and the probe used for WE connection, a small dot of silver conductive paste was placed to a corner of the substrate outside the ring.

Cyclic voltammetry (CV) was employed for the electrochemical characterization of the PEDOT:PSS/Pt NPs composite film in presence of H_2O_2 in a 900 μl solution of 1 mM H_2O_2 in Dulbecco's phosphate buffer saline (DPBS) -$CaCl_2$/-$MgCl_2$. Voltage range [−0.6, +0.6] V, scan rate of 50 mV s^{-1}, 3 cycles.

Electrochemical impedance spectroscopy (EIS) was performed with a different potentiostat (BioLogic, VSP-300) interfaced with a personal computer, equipped with the EC-Lab software. Measurements were recorded with the same three electrode setup used for other electrochemical measurements but with an Ag/AgCl pellet as reference electrode. Measurements were performed using 900 μl of DPBS -$CaCl_2$/-$MgCl_2$. The sinusoidal input signal was set to 50 mV by scanning a range of frequencies from 0.1 Hz to 1 MHz.

ENODe Steady-State Characterization and Experimental Setup: The fabricated ENODes were electrically characterized using the commercial platform ARKEO, composed by a stage and a two-channel source meter unit (SMU). Here, two channels were connected through spring contact probes to induce the field effect operation through the gate and the source and drain electrodes. Silver conductive paint was used to ensure a stable connection between the electrodes and the probes used to measure and record electrical impulses. An electrolyte solution (DPBS -$CaCl_2$/-$MgCl_2$), contained by a soft polydimethylsiloxane (PDMS) microfluidic channel (4 mm x 17 mm) positioned on top of the device, ensured ionic contact between the gate and channel.

The gate voltage (V_G) was swept from −0.2 to 0.8 V with a step of 0.05 V, while the drain voltage (V_{DS}) from -0.6 to 0.1 V with a step of 0.05 V, obtaining the output and transfer curves of the devices. The transconductance was obtained as the first derivative of channel current (I_{DS}) with respect to (V_{GS}).

ENODe Transient Response Characterization: The channel current of the OECT (I_{DS}) was measured by keeping a fixed drain potential (V_{DS} =

−200 mV), while applying square-wave pulses with a 0 V baseline and an amplitude of 0.3 V as gate potential. Each measurement consisted of six pulses with a width of 3 s and an inter-spike interval of 9 s (Δt). The sampling time used for the acquisition was set to 0.05 s. For the sake of a better visualization, the data were resampled with a sampling time of 0.3 s, so that capacitive peaks couldn't appear in channel current plots. The number of charges injected by the gate was calculated by integrating the gate current occurring during the application of the gate voltage pulse. The amount of retained charges was obtained by integrating the gate current with the removal of the pulse and subtracting this contribution from the charge injected.[34]

ENODe H_2O_2 Sensing Characterization: To assess sensing performance of Pt-functionalized ENODes, calibration curves were obtained. This approach involved the addition of H_2O_2 while the gate was constantly biased at +0.3 V. The H_2O_2 concentration in the electrolyte was raised from 50 nM to 500 μM.

Two differently diluted solutions of H_2O_2 were prepared:

1) 10 μM diluted to obtain concentrations from 50 nM to 5 μM in the microfluidic channel.
2) 1 μM diluted to obtain concentrations from 10 μM to 500 μM in the microfluidic channel.

Additions were done 5 min after current stabilization. To compare different devices a normalized current was calculated considering the channel current value 2 min after adding H_2O_2 solution for each concentration: $\frac{\Delta I}{I_0} = \frac{I_{DS}(2\text{ mins after addition}) - I_{DS}(V_G=0)}{I_{DS}(V_G=0)}$. Mean and standard deviation of this normalized current ($\Delta I/I_0$) were obtained from measurements performed on three different devices, constituting a dose-response curve, which was fitted with a sigmoid function $y = D + \frac{(A-D)}{(1+(\frac{x}{C})^B)}$, where A,B,C,D are constants, y is ($\Delta I/I_0$) and x represents H_2O_2 concentration.

ENODE neuromorphic activity characterization: The previously mentioned experimental setup and parameters for devices' transient response characterization were used consistently for neuromorphic measurements. In this case, measurements were performed with 3 different H_2O_2 concentrations (10 μM, 100 μM, and 1 mM) in the electrolyte's channel. From these ones, channel conductance percentage variations (ΔG%) for each concentration were obtained according to the following formula: $\Delta G\% = \frac{I_{END}-I_0}{I_0} \times 100$, where I_{END} represents the channel current taken after the whole pulsed measurement and I_0 represents the channel current value before the starting of the measurements.

Opto-Electronic Measurements: The opto-electronic measurements were conducted with the same setup used for the electrical characterization (ARKEO, Cicci Research S.r.l.). The device was placed on the stage with the PEDOT:PSS channel and the microfluidic PDMS channel (4 mm in width) in correspondence of a stage circular aperture (2.2 mm in diameter). Measurements were carried out simultaneously during electronic neuromorphic functioning. A squared glass coverslip was positioned on top of the PDMS microfluidic channel, so that the electrolyte could assume a flat perpendicular surface in the light path, reducing phenomena of scattering, undesired light focusing, and drift during experiments. 40 μl of electrolyte, which had the same composition used for the electrical characterization, was inserted in the microfluid channel. The light source was warm white at 15% of the maximum nominal lamp power. An integration time of 0.2 ms with a number of averaged data points equal to 100 per measurement was set. A first acquisition was made in dark conditions, without the light source. Then a reference measurement was acquired with the light source on to calculate the intensity counts of the light transmitted through the sample (Glass/Electrolyte/PEDOT:PSS film/Glass substrate/Aperture) when the device was not working. Subsequently, a measurement contemporary to an electrical one, which consists in the application of a positive gate voltage square pulse with a 0.3 V amplitude, was carried out tracking the absorbance (related to an intensity peak at a wavelength of 600 nm) variation over time.

Supporting Information

Acknowledgements

Conflict of Interest

The authors declare no conflict of interest.

Data Availability Statement

The data that support the findings of this study are available from the corresponding author upon reasonable request.

Keywords

[1] P. Gkoupidenis, Y. Zhang, H. Kleemann, H. Ling, F. Santoro, S. Fabiano, A. Salleo, Y. Van De Burgt, *Nat Rev Mater* **2023**, *9*, 134.

[2] H. Li, J. Wang, Y. Fang, *Nanoscale Adv.* **2020**, *2*, 3095.

[3] Y. Lee, T.-W. Lee, *Acc. Chem. Res.* **2019**, *52*, 964.

[4] P. Jastrzebska-Perfect, S. Chowdhury, G. D. Spyropoulos, Z. Zhao, C. Cea, J. N. Gelinas, D. Khodagholy, *Adv. Funct. Mater.* **2020**, *30*, 1909165.

[5] G.-T. Go, Y. Lee, D.-G. Seo, T.-W. Lee, *Adv. Mater.* **2022**, *34*, 2201864.

[6] T. Wang, M. Wang, J. Wang, L. Yang, X. Ren, G. Song, S. Chen, Y. Yuan, R. Liu, L. Pan, Z. Li, W. R. Leow, Y. Luo, S. Ji, Z. Cui, K. He, F. Zhang, F. Lv, Y. Tian, K. Cai, B. Yang, J. Niu, H. Zou, S. Liu, G. Xu, X. Fan, B. Hu, X. J. Loh, L. Wang, X. Chen, *Nat Electron.* **2022**, *5*, 586.

[7] R. Bhunia, E. K. Boahen, D. J. Kim, H. Oh, Z. Kong, D. H. Kim, *J. Mater. Chem. C* **2023**, *11*, 7485.

[8] Y. van de Burgt, E. Lubberman, E. J. Fuller, S. T. Keene, G. C. Faria, S. Agarwal, M. J. Marinella, A. Alec Talin, A. Salleo, *Nat. Mater.* **2017**, *16*, 414.

[9] S. T. Keene, A. Melianas, Y. Van De Burgt, A. Salleo, *Adv. Electron. Mater.* **2019**, *5*, 1800686.

[10] K. Kim, M. Sung, H. Park, T. Lee, *Adv. Electron. Mater.* **2022**, *8*, 2100935.

[11] S. T. Keene, C. Lubrano, S. Kazemzadeh, A. Melianas, Y. Tuchman, G. Polino, P. Scognamiglio, L. Cinà, A. Salleo, Y. Van De Burgt, F. Santoro, *Nat. Mater.* **2020**, *19*, 969.

[12] G. M. Matrone, E. R. W. Van Doremaele, A. Surendran, Z. Laswick, S. Griggs, G. Ye, I. McCulloch, F. Santoro, J. Rivnay, Y. Van De Burgt, *Nat. Commun.* **2024**, *15*, 2868.

[13] C. Ausilio, C. Lubrano, D. Rana, G. M. Matrone, U. Bruno, F. Santoro, *Adv. Sci.* **2024**, *11*, 2305860.

[14] L. Kergoat, B. Piro, D. T. Simon, M.-C. Pham, V. Noël, M. Berggren, *Adv. Mater.* **2014**, *26*, 5658.

[15] A. Marks, S. Griggs, N. Gasparini, M. Moser, *Adv. Mater. Interfaces* **2022**, *9*, 2102039.

[16] D. A. Bernards, D. J. Macaya, M. Nikolou, J. A. DeFranco, S. Takamatsu, G. G. Malliaras, *J. Mater. Chem.* **2007**, *18*, 116.

[17] U. Bruno, D. Rana, C. Ausilio, A. Mariano, O. Bettucci, C. Musall, C. Lubrano, F. Santoro, *Mater. Horiz.* **2024**, *11*, 2865.

[18] X. Xu, H. Zhang, L. Shao, R. Ma, M. Guo, Y. Liu, Y. Zhao, *Angew. Chem., Int. Ed.* **2023**, *62*, 202302723.

[19] C.-W. Kuo, L.-M. Huang, T.-C. Wen, A. Gopalan, *J. Power Sources* **2006**, *160*, 65.

[20] I. Gualandi, D. Tonelli, F. Mariani, E. Scavetta, M. Marzocchi, B. Fraboni, *Sci. Rep.* **2016**, *6*, 35419.

[21] D. Ohayon, V. Druet, S. Inal, *Chem. Soc. Rev.* **2023**, *52*, 1001.

[22] J. T. Friedlein, R. R. McLeod, J. Rivnay, *Org. Electron.* **2018**, *63*, 398.

[23] I. Huang, M. Clay, S. Wang, Y. Guo, J. Nie, H. G. Monbouquette, *Analyst* **2020**, *145*, 2602.

[24] J. Schultz, Z. Uddin, G. Singh, M. M. R. Howlader, *Analyst* **2020**, *145*, 321.

[25] J. Qiu, J. Cao, X. Liu, P. Chen, G. Feng, X. Zhang, M. Wang, Q. Liu, *IEEE Electron. Device Lett.* **2023**, *44*, 176.

[26] G. M. Matrone, U. Bruno, C. Forró, C. Lubrano, S. Cinti, Y. van de Burgt, F. Santoro, *Adv. Mater. Technol.* **2023**, *8*, 2201911.

[27] J. Rivnay, S. Inal, B. A. Collins, M. Sessolo, E. Stavrinidou, X. Strakosas, C. Tassone, D. M. Delongchamp, G. G. Malliaras, *Nat. Commun.* **2016**, *7*, 11287.

[28] T. Tseng, C.-F. Chang, W.-C. Chan, *Molecules* **2014**, *19*, 7341.

[29] J. J. Burmeister, V. A. Davis, J. E. Quintero, F. Pomerleau, P. Huettl, G. A. Gerhardt, *ACS Chem. Neurosci.* **2013**, *4*, 721.

[30] A. Citri, R. C. Malenka, *Neuropsychopharmacol* **2008**, *33*, 18.

[31] A. Savarimuthu, R. J. Ponniah, *Integr. Psych. Behav.* **2024**, *58*, 303.

[32] H. Liu, T. Wu, X. G. Canales, M. Wu, M-K. Choi, F. Duan, J. A. Calarco, Y. Zhang, *Sci. Adv.* **2022**, *8*, eabi9071.

[33] M. M. Pal, *Front. Hum. Neurosci.* **2021**, *15*, 722323.

[34] C. Lubrano, U. Bruno, C. Ausilio, F. Santoro, *Advanced Materials* **2022**, *34*, 2110194.